# Paleomagnetic and geochemical data from the late Miocene Lobato Formation adjacent to the Santa Clara fault system, Chili quadrangle, Rio Arriba County, New Mexico

Michael S. Petronis and Jennifer Lindline

New Mexico Geology, v. 33, n. 2 pp. 27-39, Print ISSN: 0196-948X, Online ISSN: 2837-6420.
*https://doi.org/10.58799/NMG-v33n2.27*

*This page is intentionally left blank to maintain order of facing pages.*

# Paleomagnetic and geochemical data from the late Miocene Lobato Formation adjacent to the Santa Clara fault system, Chili quadrangle, Rio Arriba County, New Mexico

*Michael S. Petronis* and *Jennifer Lindline*, Environmental Geology Program, Natural Resources Management Department, New Mexico Highlands University, P.O. Box 9000, Las Vegas, New Mexico 87701

## Abstract

New paleomagnetic and petrologic data from late Miocene volcanic rocks in the northern Española Basin of north-central New Mexico help constrain the late Tertiary tectonic history and landscape development of the area. We studied a 100-m-thick (328-ft-thick) section of the ~10 Ma Lobato Formation in Arroyo de la Plaza Larga, an east-trending drainage in the northeastern Jemez Mountains. The Lobato Formation represents some of the earliest precaldera mafic volcanism associated with the Jemez Mountain volcanic field and coincides with an episode of crustal extension in the Española Basin. At Arroyo de la Plaza Larga, Lobato Formation flows are subhorizontal for nearly 2 km (1.25 mi) southeast from their eruptive source in the Cerro Roman volcanic center. These flows take on a monoclinal geometry with an apparent northeast-trending fold axis where they flow over an erosional escarpment adjacent to the Santa Clara fault, a prominent northeast-striking structure along the western part of the Española Basin. Here we show that the apparent monocline is not of a structural origin but formed due to lava flow emplacement down an escarpment formed by displacement along the Santa Clara fault. One hundred thirty-four oriented samples were collected for paleomagnetic analysis from 16 sites from the hinge zone and east limb of the apparent monocline. Paleomagnetic data reveal a single-component magnetization that decays to the origin with less than 10% of the natural remanent magnetization remaining after treatment in 120 mT fields. In situ results from sites located in the hinge zone and those from the east fold limb yield statistically indistinguishable remanence directions. Following structural correction, based on the strike and dip of the individual flows, the dispersion between the two data sets increased, indicating failure of the fold test at the 95% confidence level. We argue that the Lobato Formation basalts from Cerro Roman were emplaced into a paleovalley of considerable relief adjacent to the Santa Clara fault and that during the late Miocene, it was an active structure that influenced the topography and drainage systems of the western margin of the Rio Grande rift.

## Introduction

The Rio Grande rift is one of the world's major late Cenozoic continental rifts extending south from at least Leadville, Colorado, to Chihuahua, Mexico. It represents the easternmost expression of widespread continental extension in the western United States during the past 30 m.y. The Rio Grande rift is characterized by normal faulting, basin formation, and predominantly mafic volcanism. The northern part of the rift is relatively narrow, consisting of an array of north-trending westward-stepping, en echelon basins separated by northeast-trending oblique accommodation zones (Rosendahl 1987; Chapin 1988).

The Española Basin, located in north-central New Mexico, is a structural depression between the eastward-tilting Nacimiento uplift and the westward-tilting Sangre de Cristo Mountains. To the north, it is separated from the Taos Plateau and the San Luis Basin by a basement ridge, which extends northwest from the Picuris Range through isolated Precambrian rock exposure at Cerro Azul to the La Madera area. The basin is bounded by the Sangre de Cristo Mountains to the east and the Precambrian-cored Nacimiento uplift to the west (Manley 1979). The western half of the basin is filled with volcanic rocks of the Jemez Mountains, which represent the western edge of the topographic basin. The basin terminates to the north near the basalts of the Servilleta Formation and to the south close to the Cerros del Rio volcanic field. Tertiary sedimentary rocks and alluvial deposits of Pliocene–Pleistocene age are preserved in the central basin and the Picuris and Abiquiu reentrants (Manley 1979).

The Española Basin is separated structurally from the San Luis Basin to the north by the Embudo fault accommodation zone (Dungan et al. 1984; Muehlberger 1979). The Embudo fault is dominated by left-lateral, northwest-down oblique slip (Muehlberger 1978, 1979; Steinpress 1980, 1981; Leininger 1982) and is considered an intracontinental transform fault (Muehlberger 1978, 1979), though components of reverse slip related to local shortening have been documented (Muehlberger 1978, 1979; Personius and Machette 1984; Leininger 1982; Kelson et al. 1997). The Embudo fault zone contains a northern strand (the La Mesita fault) with a down-to-the-northwest component and a southern strand (the Santa Clara fault) with a down-to-the-southeast component (Harrington and Aldrich 1984). Recent work indicates that the two structures are not continuous, but rather there is a structurally complicated right step between these two structures at, and east of, the south tip of Black Mesa (Koning et al. 2004b).

Although there has been substantial normal slip on the Santa Clara fault, the direction and magnitude of lateral slip is not well established. Aldrich (1986) and Aldrich and Dethier (1990) make a case for right-lateral slip. However, slickenline data from Gonzales (1993) show predominantly left-lateral slip on north-striking relatively short fault segments that link longer, northeast-striking faults with insufficient kinematic indicators. Resolving the sense and timing of movement of structures in the Española Basin is important for understanding its geologic evolution. In this paper, we present paleomagnetic and petrologic data on the Lobato Formation from the Santa Clara fault zone in the northern Española Basin that constrain timing of fault movement and further the understanding of late Neogene tectonic-volcanic activity in the north-central Rio Grande rift.

## Geologic setting

The studied Lobato Formation is part of the Miocene–Quaternary Jemez Mountains volcanic field (Bailey et al. 1969). The Jemez Mountains volcanic field is located at the intersection of the Rio Grande rift (Chapin and Seager 1975; Cordell 1978; Baldridge et al. 1983, 1984; Olsen et al. 1987) and the Jemez lineament, a broad northeast-trending alignment of late Tertiary–Quaternary volcanic centers that is interpreted to follow a Proterozoic suture zone (Mayo 1958; Aldrich 1986). The Rio Grande rift is dominated by a series of half grabens, including the Española Basin, which switch symmetry across accommodation zones throughout the north-south extent of the rift (Chapin and Cather 1994). These transverse structures have the same general northeast strike as the Jemez lineament and facilitate displacement transfer between the half grabens. Volcanic rocks of the Jemez Mountains volcanic field fill the western part of the Española Basin, which is dissected by a complicated array of normal and strike-slip faults, including the northeast-striking steeply dipping (70°) Santa Clara fault (Koning et al. 2004a, 2004b, 2005). The Santa Clara fault zone is marked by hundreds of meters of moderately to steeply southeast-dipping beds (30° to overturned) and slickenside lineaments consistently having a northward rake indicative of sinistral motion (Koning et al. 2005). The Santa Clara fault zone contains east-northeast-trending faults connected by bridge-step faults that generally strike north. Aldrich (1986) and Aldrich and Dethier (1990) argued that motion along the fault was predominantly dip slip before about 12.4 Ma to about 10 Ma and predominantly strike slip since that time. Koning et al. (2005) contended that the latest motion on the Santa Clara fault was east-down left-lateral

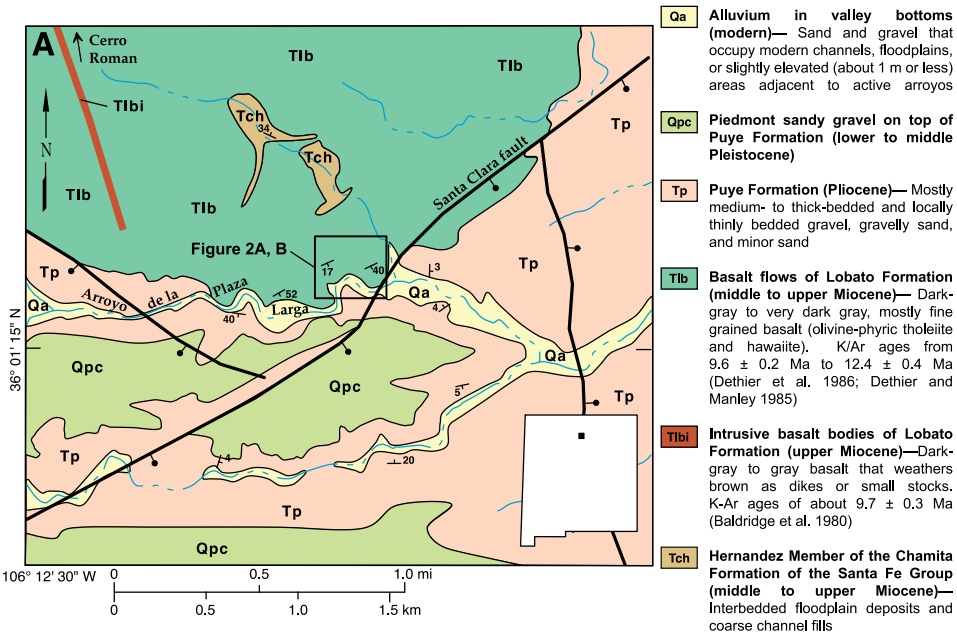


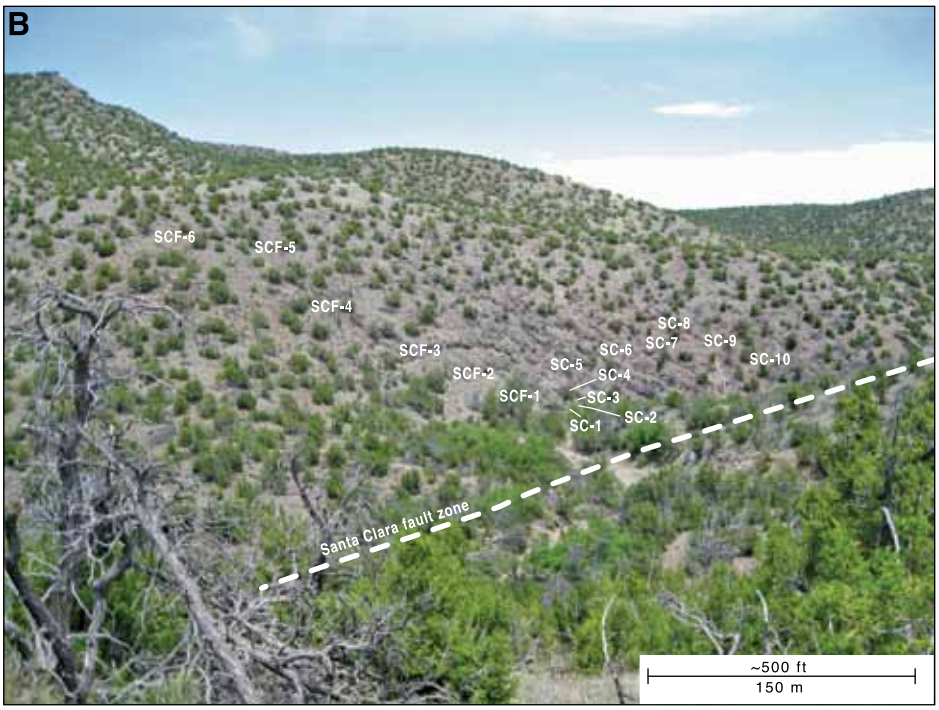


FIGURE 1—**A**—Simplified geologic map of the Arroyo de la Plaza Larga area showing the distribution of late Tertiary sedimentary, intrusive, and volcanic rocks and Quaternary deposits. Inset map shows location of study area in north-central New Mexico, (map redrawn and modified from Koning et al. 2005). **B**—View to the northeast approximately perpendicular to the apparent monocline fold axis within Arroyo de la Plaza Larga. Labels indicate approximate location of paleomagnetic sampling sites (Table 1). Dashed white line is the inferred trace of the Santa Clara fault zone.

oblique slip consistent with kinematic data from small northeast-striking fault populations in the region.

The Lobato Formation is a precaldera volcanic unit that crops out on the northern to eastern flanks of the Jemez Mountains volcanic field and forms prominent mesas throughout the area (Smith 1938). The unit consists of multiple flows and associated cinder deposits of primarily olivine basalt that yield K/Ar age determinations ranging from 14.05 ± 0.33 Ma to 7.6 ± 0.4 Ma (Dalrymple et al. 1967; Bachman and Mehnert 1978; Luedke and Smith 1978; Baldridge et al. 1980; Manley and Mehnert 1981; Aldrich 1986; Gardner et al. 1986) with a voluminous phase of volcanism occurring between 10.8 ± 0.3 Ma to 9.1 ± 0.2 Ma (Gardner et al. 1986). Lobato Formation volcanism occurred concurrently with, and was likely driven by, tectonic activity associated with Rio Grande rifting. Across the region, eruption of the Lobato Formation likely occurred from at least four vents producing a number of shield cones and possible fissure vents. Individual flows measure 2–5 m (6.5–16.5 ft) thick and interfinger locally with clastic sediments of the Santa Fe Group (Baldridge et al. 1980; Dethier and Manley 1985; Goff et al. 1989). Precaldera mafic volcanism in the Jemez Mountains volcanic field has been largely attributed to partial melting of the lithospheric mantle (Wolff et al. 2005). Most central rift (central Colorado to central New Mexico) volcanic rocks are predominantly alkaline, with some having high Ta/Ba, Nb/Ba and some having low Ta/Ba, Nb/Ba. Volcanic centers of the central rift have mixed mantle sources and show variable degrees of crustal contributions (McMillan 1998; Wolff et al. 2005).

The Cerro Roman vent, the source of the studied Lobato Formation, is located on a north-trending step in the Santa Clara fault zone (Fig. 1). Aldrich (1986) argued that extension along the fault likely facilitated the emplacement of magma and, based on the geometry of the steps, that extension along the Santa Clara fault was likely dominated by left-lateral motion in the late Miocene. Locally, Santa Fe Group sediments and Lobato Formation flows are steeply dipping to overturned along the Santa Clara fault, attesting to significant compression across the fault zone at some locations.

## Objectives

We examined a 100-m-thick (328-ft-thick) sequence of the Lobato Formation on the north side of Arroyo de la Plaza Larga (13N 3986941 392053), 3 km (1.9 mi) southeast of the Cerro Roman vent. The outcrops comprise a horizontal to gently dipping sequence that transitions to flows that dip steeply about a roughly northeast-trending axis into Arroyo de la Plaza Larga along the Santa Clara fault. The geometry of the flow defines a broad apparent monocline (Fig. 2A). Individual flow surfaces are readily identified by oxidized planes, and the flow bottoms are clearly recognized by rubble zones atop the oxidized surfaces (Fig. 2B). We hypothesize that (a) the southerly increase in dip is due to emplacement into a paleovalley adjacent to the Santa Clara fault during late Miocene time, or (b) the change in flow dip is due to postemplacement drag folding against the Santa Clara fault. To test these hypotheses, we conducted a paleomagnetic fold test. Paleomagnetic sampling sites were established in the subhorizontal hinge zone (six sites) and on the east limb (10 sites) of the north-northwest striking structure (Table 1). We sampled as many sites as possible in which we could correlate from the arroyo floor on the east-dipping limb to the hilltop where the flows dip gently within the apparent fold hinge. We confidently correlated the following flows across the apparent fold axis: SCF-1 = SC-3; SCF-2 = SC-4; SCF-3 = SC-5 (Table 1). Ten other flows were also sampled, although we could not correlate these across the fold axis because of poor

TABLE 1—Paleomagnetic data from the Lobato Formation basalts.

| Site | n/N | R | $\alpha_{95}$ | k | Dec (in situ) | Inc (in situ) | st/dip | Dec (corrected) | Inc (corrected) | VGP (in situ) lat | VGP (in situ) long | $A_{95}$ | Correlative to | UTM-13S E | UTM-13S N |
|---|---|---|---|---|---|---|---|---|---|---|---|---|---|---|---|
| **East limb** | | | | | | | | | | | | | | | |
| **SC-1** | 7/8 | 6.97 | 4.0 | 227.2 | **331.5** | **23.7** | 062, 35 E | **331.1** | **58.7** | 55.1 | 128.4 | 4.0 | * | 0392094 | 3986941 |
| **SC-2** | 5/8 | 4.94 | 4.3 | 257.8 | **332.0** | **16.8** | 062, 35 E | **332.0** | **51.8** | 52.6 | 123.6 | 3.2 | * | 0392094 | 3986941 |
| **SC-3** | 4/5 | 3.89 | 7.2 | 121.6 | **336.3** | **9.7** | 062, 35 E | **338.0** | **44.6** | 52.0 | 114.4 | 5.2 | SCF-1 | 0392094 | 3986941 |
| **SC-4** | 4/8 | 3.95 | 12.2 | 57.8 | **338.1** | **17.5** | 062, 35 E | **341.5** | **52.2** | 56.4 | 115.6 | 12.2 | SCF-2 | 0392094 | 3986941 |
| **SC-5** | 7/8 | 6.89 | 8.2 | 55.7 | **330.2** | **26.5** | 062, 35 E | **328.6** | **61.5** | 55.4 | 132.0 | 8.2 | SCF-3 | 0393090 | 3986959 |
| **SC-6** | 7/9 | 6.92 | 6.8 | 80.0 | **336.8** | **21.2** | 062, 35 E | **340.0** | **56.0** | 57.4 | 119.4 | 6.8 | * | 0392092 | 3986961 |
| **SC-7** | 6/7 | 5.80 | 12.2 | 25.9 | **333.4** | **24.6** | 062, 35 E | **334.5** | **59.6** | 56.8 | 126.5 | 9.6 | * | 0392100 | 3986971 |
| **SC-8** | 7/9 | 6.96 | 4.7 | 165.4 | **336.1** | **28.6** | 062, 35 E | **340.1** | **63.4** | 60.2 | 125.8 | 4.7 | * | 0392100 | 3986971 |
| **SC-9** | 9/10 | 8.92 | 5.1 | 109.9 | **337.8** | **23.2** | 062, 35 E | **342.1** | **57.9** | 58.8 | 119.3 | 5.1 | * | 0392115 | 3986988 |
| **SC-10** | 8/9 | 7.87 | 7.7 | 53.0 | **335.3** | **23.9** | 062, 35 E | **337.8** | **58.8** | 57.6 | 123.5 | 7.7 | * | 0392115 | 3986988 |
| **Fold hinge** | | | | | | | | | | | | | | | |
| **SCF-1** | 8/9 | 7.99 | 1.6 | 1272.3 | **336.4** | **23.5** | 039, 16 E | **341.1** | **37.4** | 58.4 | 122.3 | 1.6 | SC-3 | 0392133 | 3987003 |
| **SCF-2** | 8/8 | 7.98 | 3.2 | 299.7 | **336.5** | **18.6** | 039, 16 E | **340.3** | **32.6** | 56.3 | 119.2 | 3.2 | SC-4 | 0392127 | 3987008 |
| **SCF-3** | 10/10 | 9.96 | 3.2 | 232.2 | **342.1** | **23.1** | 039, 16 E | **347.5** | **36.1** | 61.1 | 112.3 | 3.2 | SC-5 | 0392105 | 3987006 |
| **SCF-4** | 8/9 | 7.99 | 1.9 | 872.6 | **342.3** | **20.9** | 039, 16 E | **347.2** | **33.9** | 60.1 | 110.7 | 1.9 | * | 0392106 | 3987011 |
| **SCF-5** | 7/8 | 6.94 | 6.3 | 93.1 | **337.3** | **23.0** | 039, 16 E | **342.0** | **36.8** | 58.7 | 120.7 | 6.3 | * | 0392101 | 3987029 |
| **SCF-6** | 7/9 | 6.99 | 2.8 | 479.7 | **333.7** | **12.4** | 039, 16 E | **336.2** | **26.8** | 51.7 | 119.1 | 3.2 | * | 0392081 | 3987035 |

Explanation: Site = paleomagnetic sampling site; n/N = ratio of samples used (n) for statistical calculation to samples collected (N) at each site; R= resultant vector length; Dec/Inc (in situ) = in situ declination and inclination; $\alpha_{95}$ = 95% confidence interval about the estimated mean direction, assuming a circular distribution; k = best estimate of (Fisher) precision parameter; VGP lat/long = latitude and longitude of the in situ virtual geomagnetic pole for the site; $A_{95}$ = is the radius of the 95% confidence circle about the VGP; st/dip = strike and dip of unit based on compaction fabric or flow contacts; Dec/Inc (corrected) = declination and inclination corrected for stratal dip. UTM location of site (NAD83).

exposure. We also collected petrographic and geochemical data to assist with paleomagnetic data interpretations as well as to place our study into the Jemez Mountains volcanic field petrogenetic context.

## Methods

### Field methods

Samples were collected at 16 sites using a portable, gasoline-powered drill with a nonmagnetic, diamond-tipped drill bit. Samples were oriented using both solar and magnetic compasses. Typically, from eight to 14 samples were drilled at each site over an area of approximately 10 $m^2$ with at least five strike and dip measurements obtained for each flow. The average flow dips for each section are shown in Table 1. Each core sample was cut into 2.2 cm × 2.5 cm right cylinder specimens, using a diamond-tipped, nonmagnetic saw blade with as many as four specimens obtained from each sample. All sites were situated away from faults or fractures, and precisely located using Garmin GPS model 60Csx (datum NAD83).

### Petrography

In outcrop the Lobato Formation rocks are aphanitic equigranular vesicular basalts. Vesicles range in size from 1.0 to 5.0 mm in diameter and may be filled with calcite. In thin section the rocks are gray to very dark gray, mostly fine-grained plagioclase ± olivine ± pyroxene porphyritic basalts. Plagioclase phenocrysts are tabular, unaltered, and measure as much as 3.0 mm in length. The olivine and pyroxene phenocrysts measure 1.0–2.0 mm in diameter. They are equant to slightly elongated crystals that have been pervasively altered to orange-red opaque minerals (iddingsite). The groundmass comprises framework plagioclase laths and intergranular olivine + pyroxene + magnetite. The magnetite is present as very fine grained (<0.10 mm diameter) equant and blocky crystals disseminated throughout the groundmass.

### Geochemistry

The bulk rock chemistry of six Lobato Formation samples was determined by Activation Laboratories, Ltd., Ontario, Canada. Data are presented in Table 2 and Fig. 3. Samples were digested by fusion with $LiBO_2$ then analyzed for major and trace elements by ICP-MS. Results show a precision of < ± 1.5% for all major elements and ± 5–10% for trace elements. Samples show a range of loss on ignition values (1.19–3.65 wt %), signifying modest to moderate secondary alteration. The chemical analyses were therefore normalized to a volatile-free basis on the major element variation diagrams to correct for the effects of hydration.

### Paleomagnetism

Remanent magnetizations of all samples were measured using an AGICO JR6A Dual Speed Spinner Magnetometer at the New Mexico Highlands University (NMHU) Paleomagnetic-Rock Magnetism Laboratory. Specimens were progressively alternating-field (AF) demagnetized, typically in 10 to 15 steps to a maximum field of 120 mT (millitesla) using an ASC Scientific D-tech 2000 AF demagnetizer. Samples with high coercivity were treated with thermal demagnetization to a maximum of 590°C, with most samples being fully demagnetized between 560° to 580°C. Thermal demagnetization on duplicate specimens, to compare with AF behavior, was conducted with a Schonstedt TSD-1 thermal demagnetizer. Principal component analysis (Kirschvink 1980) was used to determine the best-fit line through selected demagnetization data points for each sample (Table 1). For most samples, a single best-fit line could be fit to the demagnetization steps. Best-fit magnetization vectors involved five to 12 data points, but as few as three to as many as 15 were used. Magnetization vectors with maximum angular deviation values greater than



FIGURE 2—Field photographs of the Arroyo de la Plaza Larga apparent monocline. **A**—View to the north. Near the left center of the photo note the gently dipping flows within the hinge zone of the monocline; average attitude of the flow is 039°, 16°SE. The right side of the photo shows the moderately dipping flows of the east limb of the monocline; average attitude of the flows 062°, 35°SE. Dashed line is the inferred fold axis of the apparent monocline. Juniper for scale. **B**—Contact between flows defined by oxidized flow tops and rubble zone at the base of each flow.

5° were not included in site mean calculations. For less than 10% of the demagnetization results, it was necessary to anchor the magnetization vector to the origin. Individual sample directions were considered outliers and rejected from the site mean calculation if the angular distance between the sample direction and the estimated site mean exceeded 18°.

### Rock magnetism

To characterize the magnetic mineralogy, we conducted a suite of rock magnetic experiments with the principal goal of identifying the mineral phase(s) that carry the overall remanence and the quantity, composition, and grain size of the magnetic phase(s) present. Rock magnetic experiments included (1) analysis of low-field susceptibility versus temperature, (2) isothermal remanent magnetization (IRM) and backfield IRM experiments (coercivity of remanence), and (3) measurement of room temperature susceptibility in variable applied fields. All susceptibility experiments were measured with an AGICO MFK1-A kappabridge susceptibility meter, and isothermal magnetizations were imparted using an in-house built static impulse magnet at the NMHU laboratory.

Continuous low-field susceptibility versus temperature measurements were carried out in a stepwise heating/cooling fashion from 25°C to 700°C to 40°C in an argon atmosphere using a CS4 furnace attachment for MFK1-A. These experiments allow for an evaluation of the magnetic mineral composition based on Curie-point estimates and assist with revealing mixtures of magnetic phases within a given sample. An IRM acquisition experiment involved stepwise exposure to progressively stronger applied fields along the z-axis using a static impulse magnet until saturation was obtained. The shapes of the IRM curves provided information on magnetic grain size and composition. Backfield SIRM demagnetization involved applying an increasing field along the negative z-axis until the sign changed (coercivity of remanence). Room temperature susceptibility experiments in variable fields were conducted to evaluate the susceptibility dependence on direct current (DC) applied fields from 2 A/m to 700 A/m.

## Results

### Geochemistry results

The basalts are mildly alkaline in composition, like other Jemez Mountains mafic volcanic rocks (Wolff et al. 2005) as demonstrated on the total alkalies versus silica discriminant diagram (Fig. 3A). They fall within the sodic series of the alkali olivine basalt scheme, and classify as alkali basalts according to the Irvine and Baragar (1971) conventions. These flows are chemically similar to other Lobato Formation flows (Aldrich and Dethier 1990) and form some of the lower silica and higher alkaline composition of Jemez volcanic rocks. The studied Lobato Formation shows a narrow range of silica values, as demonstrated on Harker variation diagrams (Fig. 3B). It is noted, however, that the Lobato Formation at other locations includes dacitic (Goff et al. 1989) and rhyodacite (Singer and Kudo 1986) compositions and has been correlated with early (7.5 Ma) El Rechuelos Rhyolite (Loeffler et al. 1988). Most major element oxides, like CaO, show minor variation with changing MgO values, which is consistent with the similar major mineralogy within the sample set. Mobile elements, like Ba (average 611 ppm), Sr (average 725 ppm), and Rb

TABLE 2—Whole rock geochemistry of Arroyo de la Plaza Larga Lobato Formation.

| | SCF-1 | SCF-2 | SCF-3 | SCF-4 | SCF-5 | SCF-6 |
|---|---|---|---|---|---|---|
| **$SiO_2$ (wt%)** | 47.29 | 48.02 | 47.91 | 48.55 | 48.27 | 48.04 |
| **$Al_2O_3$** | 16.64 | 16.91 | 16.73 | 16.34 | 15.80 | 16.66 |
| **$FeO_{(meas)}$** | 3.12 | 1.97 | 1.78 | 3.46 | 4.22 | 3.56 |
| **$Fe_2O_{3(calc)}$** | 8.58 | 9.84 | 9.74 | 7.96 | 6.67 | 7.98 |
| **MnO** | 0.16 | 0.16 | 0.15 | 0.16 | 0.16 | 0.16 |
| **MgO** | 4.01 | 3.77 | 4.19 | 5.63 | 5.95 | 4.67 |
| **CaO** | 9.54 | 9.74 | 9.85 | 9.63 | 10.03 | 9.72 |
| **$Na_2O$** | 3.43 | 3.48 | 3.30 | 3.30 | 3.35 | 3.35 |
| **$K_2O$** | 1.05 | 1.00 | 0.86 | 0.90 | 0.88 | 0.83 |
| **$TiO_2$** | 1.67 | 1.71 | 1.65 | 1.60 | 1.54 | 1.60 |
| **$P_2O_5$** | 0.45 | 0.46 | 0.43 | 0.41 | 0.49 | 0.39 |
| **LOI** | 2.37 | 2.56 | 3.65 | 1.51 | 1.19 | 1.77 |
| **$CO_2$** | 0.53 | 0.32 | 0.65 | 0.29 | 0.62 | 0.19 |
| **$H_2O^+$** | 1.40 | 1.70 | 2.00 | 0.70 | 0.50 | 1.40 |
| **$H_2O^-$** | 0.70 | 1.20 | 1.20 | 0.40 | 0.30 | 0.70 |
| **Total** | **98.57** | **100.28** | **100.45** | **99.33** | **98.78** | **99.25** |
| **Ba (ppm)** | 580.0 | 577.0 | 614.0 | 613.0 | 719.0 | 565.0 |
| **Co** | 39.7 | 40.4 | 38.4 | 38.8 | 39.5 | 40.5 |
| **Cr** | 235.0 | 247.0 | 231.0 | 230.0 | 234.0 | 229.0 |
| **Cu** | 65.0 | 68.0 | 67.0 | 68.0 | 68.0 | 71.0 |
| **Ni** | 96.0 | 112.0 | 113.0 | 101.0 | 104.0 | 89.0 |
| **Sr** | 741.0 | 755.0 | 746.0 | 708.0 | 709.0 | 692.0 |
| **V** | 263.0 | 249.0 | 232.0 | 232.0 | 230.0 | 246.0 |
| **Y** | 24.0 | 25.0 | 23.0 | 23.0 | 25.0 | 23.0 |
| **Zn** | 79.0 | 83.0 | 81.0 | 81.0 | 80.0 | 83.0 |
| **Ga** | 17.0 | 17.0 | 17.0 | 16.0 | 20.0 | 16.0 |
| **Hf** | 3.2 | 3.1 | 3.0 | 3.0 | 3.3 | 3.1 |
| **Nb** | 17.7 | 16.9 | 16.3 | 15.5 | 15.6 | 15.3 |
| **Rb** | 13.0 | 9.0 | 4.0 | 6.0 | 7.0 | 6.0 |
| **Ta** | 1.1 | 1.1 | 1.0 | 0.9 | 1.2 | 0.9 |
| **Th** | 2.4 | 2.3 | 2.3 | 2.2 | 2.3 | 2.2 |
| **U** | 1.1 | 1.0 | 0.8 | 0.7 | 0.6 | 0.7 |
| **Zr** | 117.0 | 112.0 | 103.0 | 108.0 | 134.0 | 118.0 |
| **La** | 25.3 | 25.4 | 25.0 | 23.6 | 22.4 | 22.5 |
| **Ce** | 49.3 | 50.2 | 49.1 | 45.6 | 44.1 | 43.7 |
| **Pr** | 5.9 | 6.1 | 5.9 | 5.5 | 5.6 | 5.3 |
| **Nd** | 23.3 | 24.1 | 23.5 | 22.0 | 22.3 | 21.0 |
| **Sm** | 5.0 | 5.2 | 5.0 | 4.8 | 4.9 | 4.7 |
| **Eu** | 1.6 | 1.7 | 1.6 | 1.5 | 1.6 | 1.5 |
| **Gd** | 4.6 | 4.8 | 4.7 | 4.4 | 4.9 | 4.4 |
| **Tb** | 0.8 | 0.8 | 0.8 | 0.8 | 0.8 | 0.8 |
| **Dy** | 4.5 | 4.6 | 4.5 | 4.3 | 4.6 | 4.3 |
| **Ho** | 0.9 | 0.9 | 0.9 | 0.9 | 0.9 | 0.9 |
| **Er** | 2.4 | 2.5 | 2.4 | 2.4 | 2.5 | 2.4 |
| **Tm** | 0.3 | 0.4 | 0.4 | 0.3 | 0.4 | 0.4 |
| **Yb** | 2.2 | 2.3 | 2.2 | 2.2 | 2.2 | 2.2 |
| **Lu** | 0.3 | 0.3 | 0.3 | 0.3 | 0.3 | 0.3 |

Table 2 note: Total iron was reported as $Fe_2O_3$. $FeO_{(meas)}$ was measured through titration according to the methods of Wilson (1955). $Fe_2O_{3(calc)}$ was calculated from the difference between $Fe_2O_3$ and $FeO_{(meas)}$. $CO_2$ was determined coulometerically and $H_2O^+/H_2O^-$ was determined gravimetrically. A 0.3 g sample was thermally decomposed in a resistance furnace in a pure nitrogen environment at 110°C (moisture, $H_2O^-$) followed by decomposition at 1,000°C (interstitial water, $H_2O^+$) using an ELTRA CW-800.

(average 8 ppm) show typical values for Lobato basalts (Gardner et al. 1986; Wolff et al. 2005), suggesting little to no loss from postemplacement alteration. However, most immobile trace elements, like Ni, show a wide variation in values suggesting their fractionation within major phases. The studied samples plot as within-plate basalts on the tectonic discrimination diagram of Pearce and Cann (1973). On a Pearce (1983) multi-element diagram, the basalts show enrichment in incompatible elements, especially Ba and Th, relative to modern mid-ocean ridge basalts (MORB), which is typical of mantle melts that have erupted in within-plate settings and interacted with continental lithosphere (Fig. 3). The basalts yield low Nb/Ba and Ta/Ba ratios, indicative of an arc-like source region (McMillan 1998) wherein Nb and Ta were retained in the slab during melting. Regional lavas having similar trace element characteristics are thought to have formed from source regions established during Proterozoic craton development and affected by slab fluids (McMillan 1998; Baldridge 2004).

The basalts also show enrichment in the light rare earth elements relative to the middle and heavy rare earth elements (Fig. 3). This pattern demonstrates the evolved nature of the melt relative to chondrite, as well as the fractionation of orthopyroxene and clinopyroxene as these minerals tend to deplete the parent lava in the middle and heavy rare earth elements and enrich it in the light rare earth elements. Pearce element ratios were calculated to test for fractional crystallization using the procedures of Russell and Nicholls (1988) and Russell and Stanley (1990). The combination of fractionating phases of olivine, clinopyroxene, and plagioclase shows a slope of 0.989 and supports fractionation of these phases to explain the variation in major element oxides (Fig. 3D).

### Paleomagnetic results

**General demagnetization behavior—**All 16 sample sites in the Lobato Formation yield interpretable results (Table 1). Overall, progressive alternating-field demagnetization response of all rocks yield high quality results (Fig. 4), with a linear trajectory on vector diagrams defined over a broad

*Text continued on page 33, column 3.*

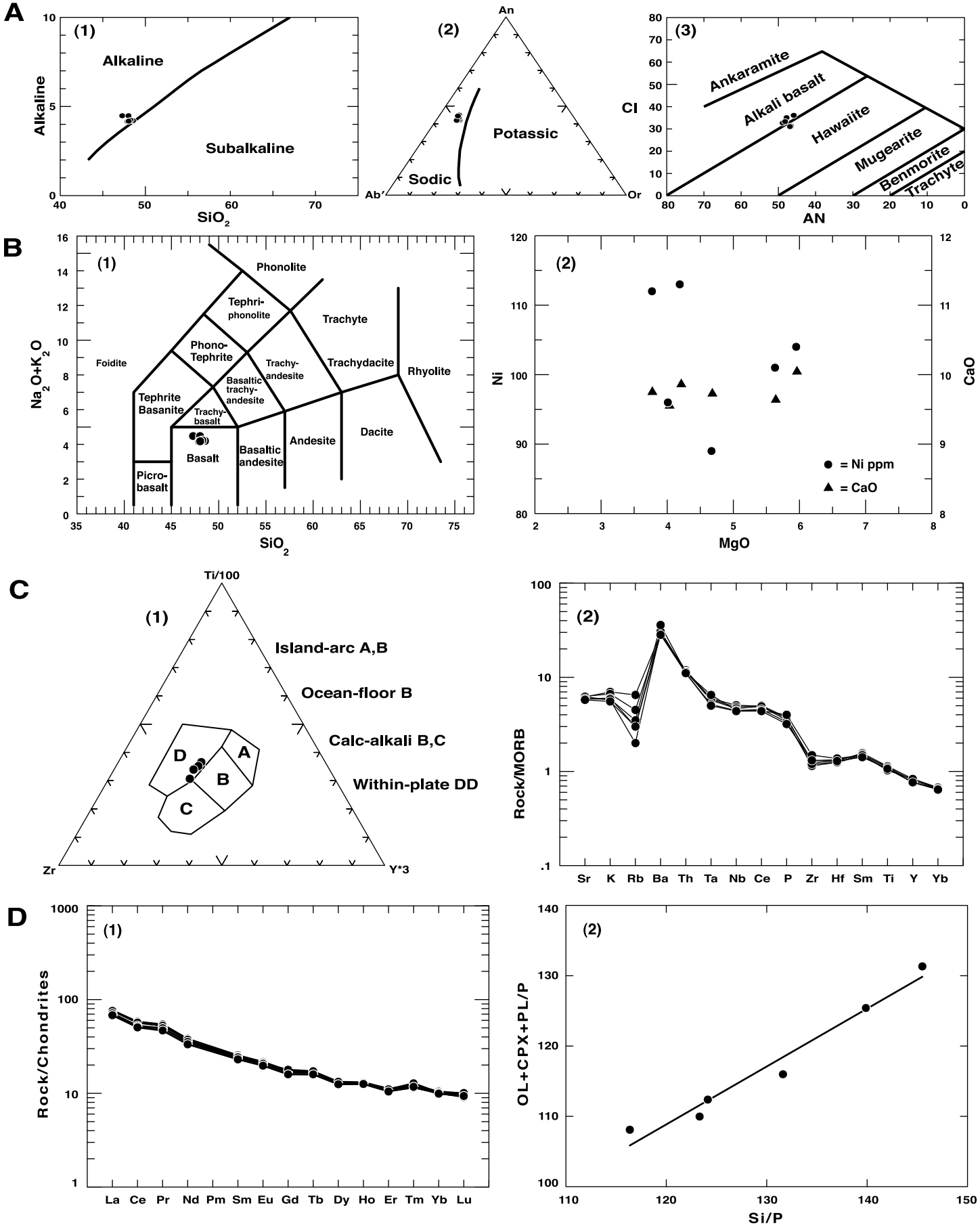


*Figure 3 caption at bottom of page 33.*

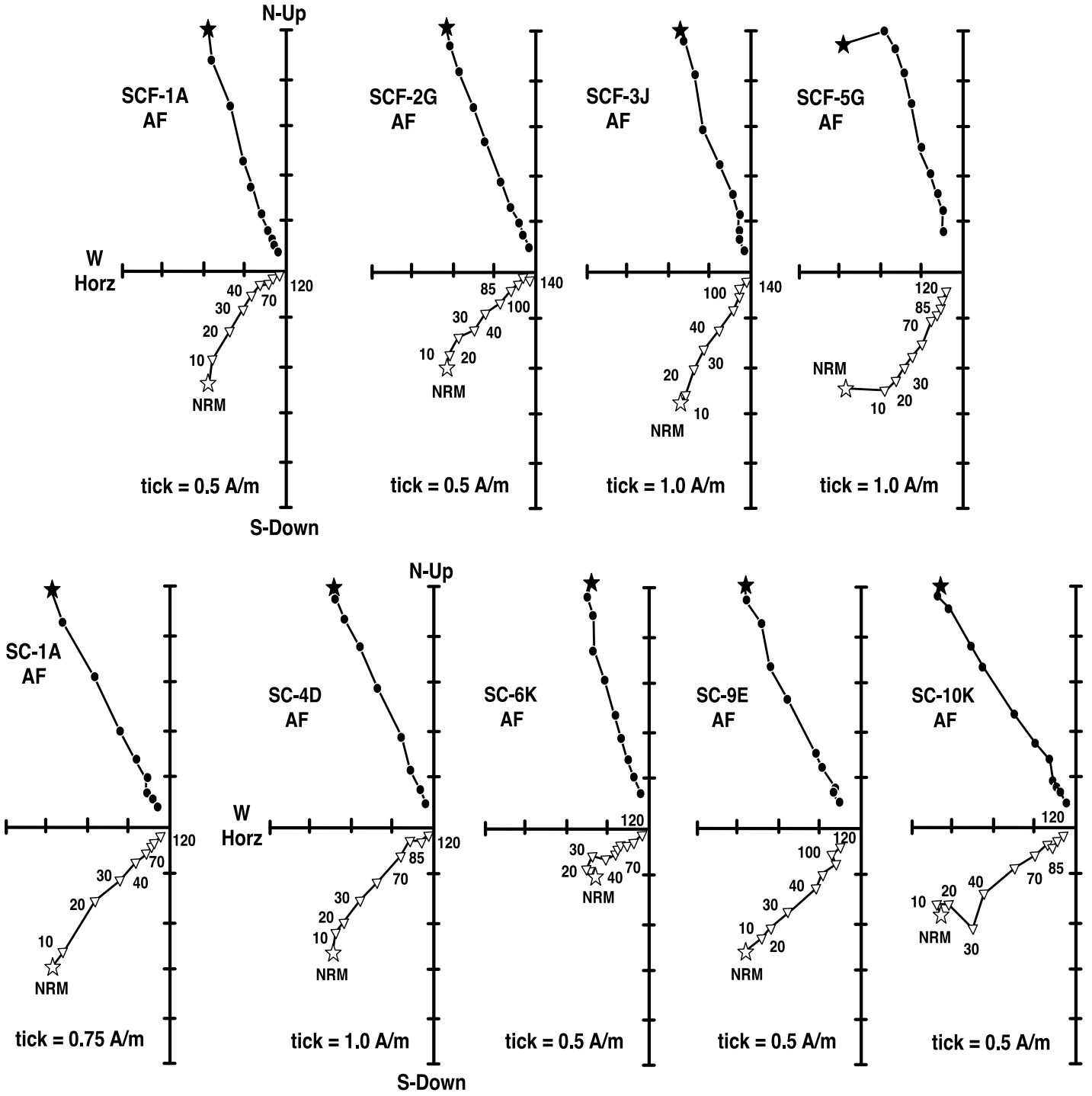


FIGURE 4—Representative in situ modified demagnetization diagrams (Zijderveld 1967; Roy and Park 1974). Solid black circles represent the projection onto the horizontal plane. Open triangles represent the projection onto the true vertical plane. AF demagnetization steps are given in millitesla. Diagrams are designated by a site number (e.g., SC-10, SCF-6) and method of treatment. Intensity (A/m) is shown along one axis for each sample; each tick equals indicated intensity.

FIGURE 3—Geochemical data for the Arroyo de la Plaza Larga Lobato flows. All major oxides in wt %. **A**—Samples are (1) alkaline in composition and (2) part of the sodic series of the (3) alkali olivine basalt scheme. Diagrams after Irvine and Baragar (1971). **B**—Geochemical variation diagrams. (1) All samples show a low and narrow range of silica values and plot within the basalt field. (2) Across the MgO spectra, the basalts show little variation in CaO but variable Ni values. **C**—(1) Tectonic discrimination diagrams after Pearce and Cann (1973) showing that all basalts plot in the "within-plate" field. (2) Multi-element variation diagrams after Pearce (1983) show enrichment in incompatible elements (e.g., Ba and Th) relative to MORB, typical of mantle melts that have erupted in within-plate settings and interacted with continental lithosphere. The low Nb/Ba and Ta/Ba ratios are indicative of an arc-like source region. **D**—(1) Rare earth element concentrations compared to those of chondrites. Normalization factors of Nakamura (1974). (2) Data plotted using Pearce element ratios. The strong trend supports fractionation of olivine, clinopyroxene, and plagioclase phases during crystallization.

*Text continued from page 31, column 3.*

range of peak fields. Duplicate specimens treated with thermal (TH) demagnetization yield directional data similar to those resolved in AF demagnetization with maximum unblocking temperatures from 560°C to 590°C for all samples. In general, most samples contain a single characteristic remanent magnetization (ChRM) that is well grouped at the site level, but some

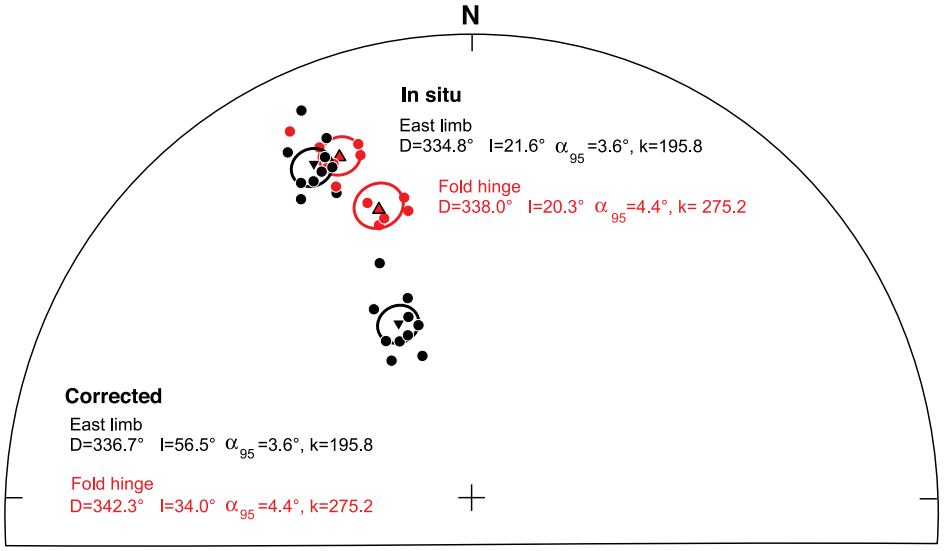


FIGURE 5—Equal area lower hemisphere projection of in situ and corrected site mean paleomagnetic directions. Black circles are site mean results from the east limb, and black triangles with 95% confidence ellipse are group mean results from the east limb. Red circles are site mean results from the fold, hinge and red triangles with 95% confidence ellipse are group mean results from the fold hinge. In situ data statistically overlap and are indistinguishable at the 95% level. Upon unfolding, the corrected data are statistically distinguishable at the 95% level indicating a negative fold test.

samples also contain additional magnetizations that are readily randomized by 10 mT or by 250°C (Fig. 4). We interpret these magnetization components as low-coercivity viscous overprints (VRM). After removing the VRM, the ChRM, which we interpret as the primary thermal remanent magnetization (TRM), decays along a roughly univectoral path to the origin with less than 10% of the natural remanent magnetization (NRM) intensity remaining after treatment in 120 mT fields or by 590°C (Fig. 4).

**Lobato Formation paleomagnetic behavior**—The basalt flows yield median destructive fields (MDF) between 50 mT and 80 mT, and this behavior is characteristic of pseudo-single domain (PSD) to single domain (SD) magnetite. All samples were fully demagnetized, with the ChRM isolated during thermal demagnetization between 560°C and 590°C, implying that a cubic phase, likely low-Ti magnetite, carries the remanence. In general, the demagnetization data from each flow are characterized by a single component, stable end-point response yielding well-defined normal polarity magnetizations. The in situ results for the 10 flows located on the east limb provide a group mean of D = 334.8°, I = 21.6°, $\alpha_{95}$ = 3.6°, k =195.8 10/10, which is statistically indistinguishable from the six flows located in the apparent hinge of the flow that yield a group mean of D = 338.0°, I = 20.3°, $\alpha_{95}$ = 4.4°, k = 275.2, 6/6 (Fig. 5). Both directions are distinct to a mid-Miocene expected normal polarity field direction (358.8°, 58.7°, $A_{95}$ = 6.3°) (Mankinen et al. 1987). After correcting for the average dip of the flows, the east limb provides a corrected group mean of D = 336.7°, I = 56.5°, $\alpha_{95}$ = 3.6°, k = 195.8 which is statistically distinct from the six flows located in the hinge of the flow, D = 342.3°, I = 34.0°, $\alpha_{95}$ = 4.4°, k = 275.2 (Fig. 5). The increase in dispersion upon 100% unfolding implies a negative paleomagnetic fold test (see discussion).

### Rock magnetism results

**Continuous susceptibility versus temperature results**—All samples are irreversible on the cooling curve (Fig. 6) with inferred Curie points between 577°C to 582°C using either the Hopkinson Peak (Moskowitz 1981) or inflection point methods (Tauxe 1998). These temperatures are consistent with a low Fe-Ti oxide phase. On heating, some samples show a slight increase followed by a decrease ("bump") in susceptibility over the interval from 200°C to 400°C, which is not present on the cooling curve (Fig. 6). This pattern is suggestive of the presence of a second ferromagnetic phase and the nonreversibility of the curves indicates that a mineralogical change occurred during the experiment (Özdemir and O'Reilly 1981, 1982). The "bump" in susceptibility on the heating curve is commonly interpreted to reflect the homogenization of two exsolved Fe-Ti oxide phases into a single titanomaghemite phase, although this process is not well understood (Hrouda 2003; Petronis et al. 2011). All curves yield a lower susceptibility on the cooling curve, which may reflect that the magnetic fraction is being altered by heating, resulting in a phase with a lower susceptibility. Hrouda (2003) concludes that the nature of this alteration is difficult to fully characterize, yet these results are typically interpreted to indicate that the magnetic mineral that homogenizes is titanomaghemite (Özdemir and O'Reilly 1981, 1982). Moreover, Hrouda (2003) points out that the lower susceptibility during the cooling cycle may result from (1) the inversion of titanomaghemite to titanium-poor magnetite and ilmenite during heating and/or (2) the reduction of these phases to form titanomagnetite. Alternatively, the lower susceptibility on the cooling is simply an artifact of the measurement procedure controlled by the oxygen fugacity of the oven.

**IRM and BIRM experiments**—IRM acquisition curves show a narrow spectrum of responses that indicate the samples are likely dominated by a cubic phase (magnetite-type curves) (Fig. 7). All samples show steep acquisition and reach near saturation by 0.30 T–0.35 T (tesla) and show no evidence of a high coercivity phase on treatment to maximum applied fields of 2.5 T. The acquisition curves are characteristic of PSD- to SD-magnetite-dominated behavior that is influenced by somewhat higher-coercivity SD magnetite and, on the basis of other observations (unblocking temperature spectra during thermal demagnetization of the NRM), some titanomaghemite. Backfield IRM curves yield coercivity of remanence values between 0.06 T and 0.10 T consistent with a low Ti magnetite phase (Fig. 7).

**Room temperature susceptibility in variable applied fields**—Bulk susceptibility was measured in 20 steps in applied fields from 2 A/m to 700 A/m. All samples show a very moderate dependence on applied field intensity (Fig. 8). SC-2 yields a slightly more field dependence, indicating a minor compositional variation from the other samples that reflects a higher Ti content of the oxide phase. Average bulk susceptibility ranges from 0.007 SI to 0.02 SI, which are typical values for mafic igneous rocks (Fig. 8). SC-2 yields the highest susceptibility (0.02 SI) consistent with the above observation of a slight compositional difference relative to the other samples.

## Discussion

The Española Basin was tectonically and volcanically active during the middle Miocene. Cerro Roman is one of many eruptive centers in the southern Española Basin that tapped fertile continental lithosphere in response to Rio Grande rift extension. Our data sets shed insight into the vertical displacement across the Santa Clara fault at the time of the eruption.

### Paleomagnetic fold test

The paleomagnetic fold test (Cox and Doell 1960) evaluates the relative timing of acquisition of a component of the NRM, typically the ChRM, and allows for an assessment of the timing of folding (Everitt and Clegg 1962; Butler 1992). If a ChRM was acquired before folding, directions of ChRM from sites on opposing limbs of a fold are dispersed when plotted in geographic coordinates (in situ)

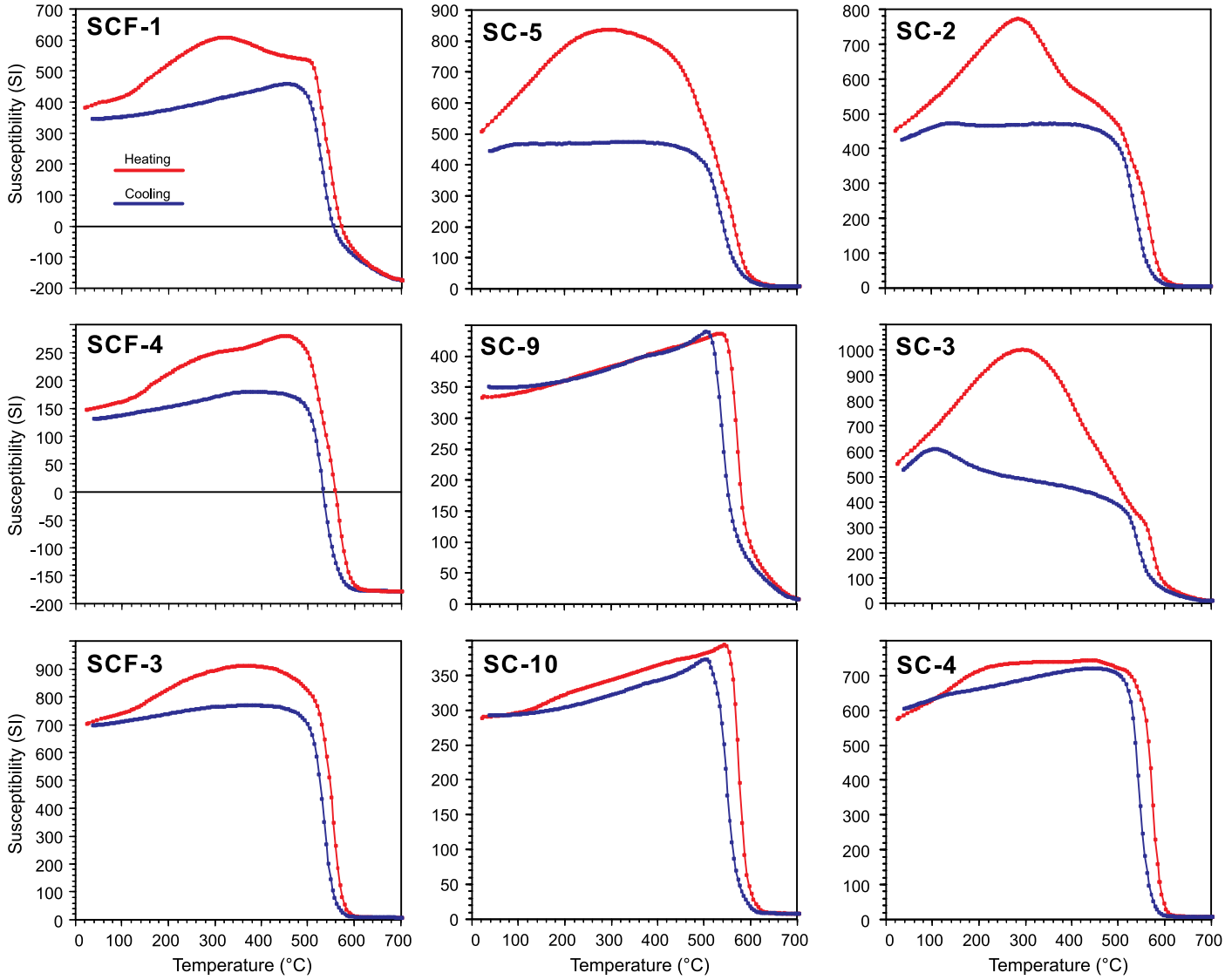


FIGURE 6—Continuous low-field susceptibility versus temperature experiments from 25°C to 700°C and cooling to 40°C. Susceptibility (in SI) are absolute values corrected for the diamagnetic quartz sample holder.

but converge when the structural correction is made (Fig. 9A). The ChRM directions are said to "pass the fold test" if, after applying the structural correction, the clustering increases with an associated decrease in the data dispersion parameter (Fig. 9B). Alternatively, the data are said to "fail the fold test" if the ChRM directions become more scattered with an associated increase in data dispersion parameter. Following these guidelines, the data from the Lobato Formation fail the fold test.

Our two hypotheses to explain the apparent monoclinal fold geometry of the Lobato Formation flows are either that the flows were erupted down a slope into a paleovalley or were folded due to drag along the Santa Clara fault. The paleomagnetic fold test demonstrates (Fig. 5) that when this sequence of basalts erupted, a paleovalley existed adjacent to the Santa Clara fault. It is probable that left-oblique motion of the Santa Clara fault resulted in southeast-side-down motion of the hanging-wall block and formed a topographic depression into which the Lobato Formation flowed. Stratigraphic and structural studies in Santa Clara Canyon, a drainage located approximately 5 km (3 mi) to the west of Arroyo de la Plaza Larga, indicate that it, too, preserves a basalt-filled paleovalley (Aldrich and Dethier 1990). In Santa Clara Canyon, the Lobato Formation forms a thick (> 200 m; >656 ft) section of flows on the north wall; but they are completely absent on the south wall. The absence of a fault contact at Santa Clara Canyon and the interlayering of the Lobato Formation with the fluvial Tesuque Formation indicate that a drainage channel also existed in the area of Santa Clara Canyon in the middle Miocene (Aldrich and Dethier 1990).

An alternative explanation of the paleomagnetic data is that the Lobato basalts were remagnetized after being folded against the Santa Clara fault. If that were the case, the dispersion of the data after unfolding is an artifact of the remagnetization event. Several factors, however, suggest that the ChRM is a primary TRM. The rock magnetic data and demagnetization behavior are typical of little-altered basaltic lava flows rather than chemically remagnetized rocks. Demagnetization behavior of all samples shows a single component magnetization on vector diagrams that decays linearly to the origin with no evidence of secondary components (Fig. 6), and alternating-field demagnetization curves are consistent with a magnetically hard TRM carried by SD to PSD grains rather than a weak-field IRM or VRM typical of magnetically soft secondary phase (Dunlop and Özdemir 1997). Isothermal remanent magnetization acquisition experiments yield steep, rapid saturation by 0.3 T to 0.35 T fields sufficient to fully saturate elongate SD magnetite and maghemite grains (Fig. 7). The Curie-point estimates are typical of low-Ti titanomagnetite grains

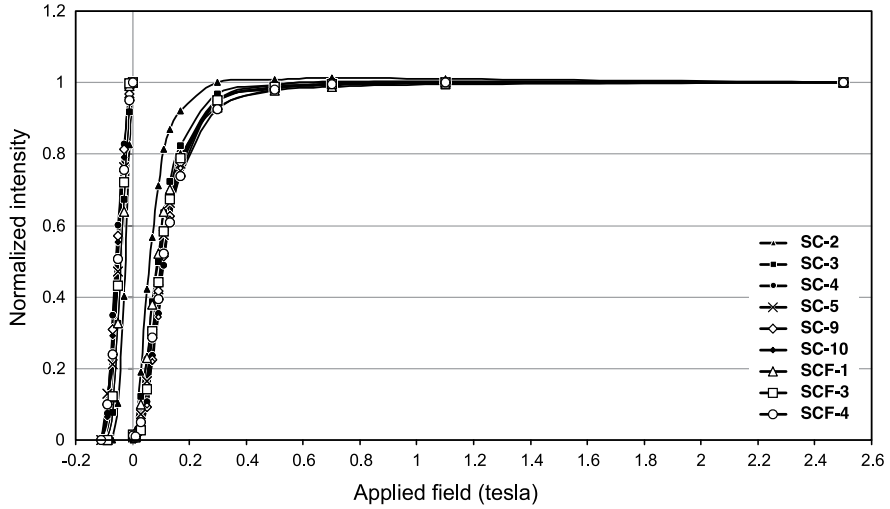


FIGURE 7—Representative normalized isothermal remanent magnetization (IRM) acquisition and backfield IRM demagnetization curves from representative samples. All samples reach saturation between 0.30 T and 0.35 T, indicating the presence of cubic low-Ti magnetite and/or titanomagnetite phase. Backfield IRM curves yield coercivity of remanence values between 0.06 T and 0.10 T.

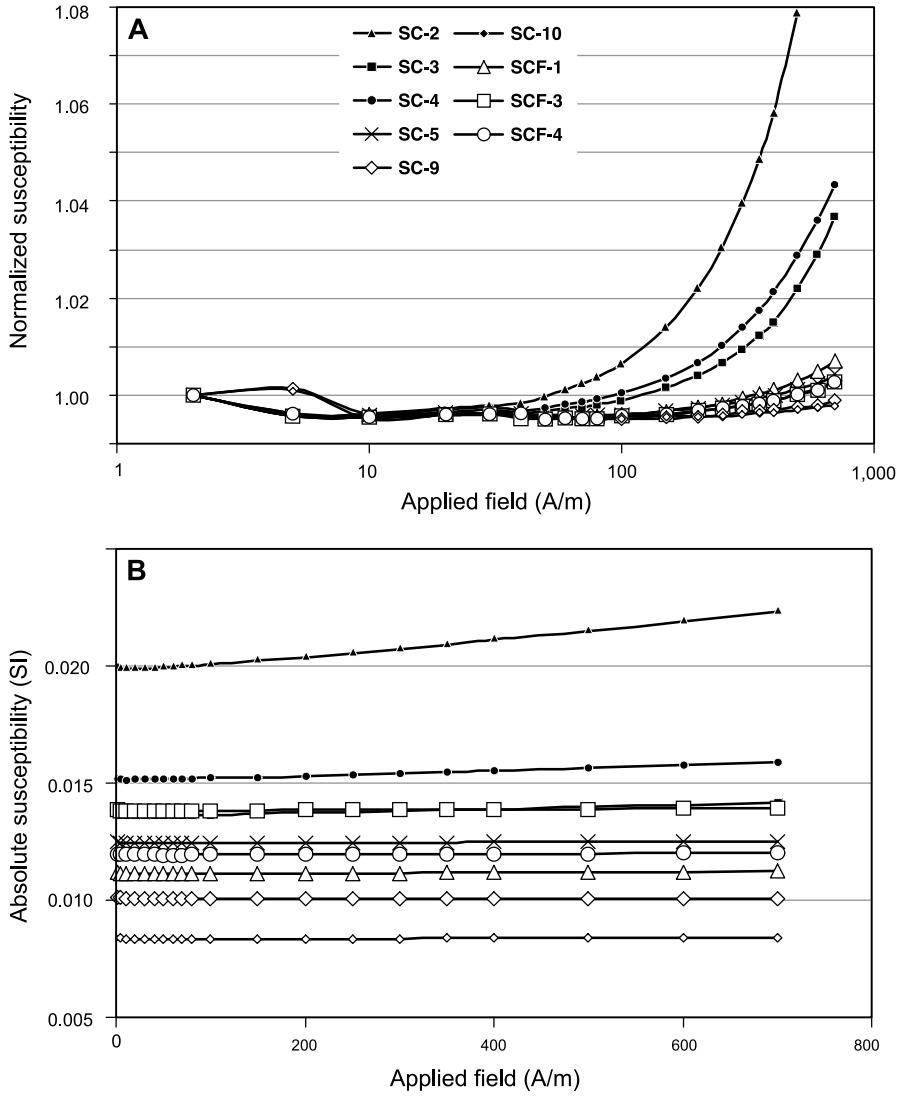


FIGURE 8—Low-field susceptibility versus applied fields from 2 A/m to 700 A/m (ampere/meter). **A**—Low-field susceptibility results normalized to the 300 A/m applied field. All samples show only small susceptibility dependence with applied fields. SC-2 shows a somewhat stronger dependence, indicating a slight compositional difference with respect to the other samples. **B**—Absolute susceptibility results. SC-2 yields a slightly higher absolute susceptibility magnitude.

from unaltered basalt (Fig. 8). In addition, the whole-rock and trace element geochemical data further support the case for a primary TRM as the results show no evidence of hydrothermal alteration because elements like Ba, Sr, and Rb, which are highly fluid mobile, remain at typical values for unaltered basalts.

Additional support for a primary TRM comes from comparison to a paleomagnetic study of the Lobato Formation by Brown and Golombek (1985). Brown and Golombek (1985) sampled the Lobato Formation at seven sites from the northeastern part of the Jemez Mountains volcanic field and two sites near Chili, New Mexico. The two sites near Chili did not yield stable end-point behavior during demagnetization and were not included in the final group mean. The remaining sites (seven) yielded a generally stable behavior during demagnetization with no indication of secondary magnetization components. Median destructive fields were around 20 mT for all samples and within-site dispersion low (Brown and Golombek 1985). The seven accepted sites yielded a normal polarity group mean of D = 004.5°, I = 51.8°, $\alpha_{95}$ = 13.5°, k = 21; however, individual site mean directions are somewhat scattered ranging from D = 325.2°, I = 36.9° to D = 029.0°, I = 59.0°. As the sampling sites were located on a series of fault blocks with variable displacement sense, Brown and Golombek (1985) attributed the relatively large scatter between sites to the lack of correction for tilt. The 16 sites collected from the Lobato Formation in our study yield demagnetization behavior and directional data consistent with a primary TRM and with the demagnetization response of Brown and Golombek (1985), who also argued for a primary TRM (Fig. 5; Table 1). Based on these similarities, we argue that it is unlikely that the northern to northeastern part of the Jemez Mountains volcanic field, including the Lobato Formation, experienced a pervasive remagnetization event. Rather, the ChRM of the sites in this study carry a primary TRM and can be used to evaluate the emplacement of the Lobato Formation flows. Various other paleomagnetic studies on the Santa Fe Group and igneous rocks from the Española Basin and surrounding area demonstrate that these rocks carry a primary remanence further refuting a pervasive regional remagnetization event (Barghoorn 1981; Brown and Golombek 1986; Salyards et al. 1994; Hudson et al. 2004; Harlan and Geissman 2009).

### Paleotopography

The Santa Clara fault forms as a major boundary zone between two different regions of the Española Basin. To the northwest, the Abiquiu embayment lies between the Embudo fault system and Santa Clara faults to the east and several

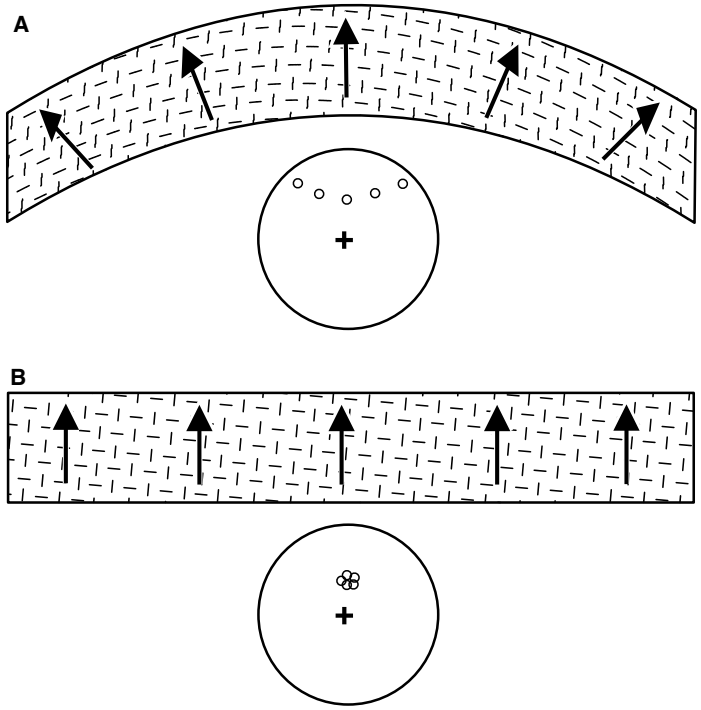


FIGURE 9—Schematic diagram of the fold test of paleomagnetic stability. **A**—Upper diagram: Bold arrows are in situ directions of the characteristic remanent magnetization (ChRM) in limbs of the fold. Lower diagram: Equal-area lower hemisphere projection shows the in situ ChRM directions across the fold. **B**—Example of ChRM directions that pass the fold test. Improved grouping of the ChRM upon restoring the limbs of the fold to horizontal indicates that the ChRM was acquired before folding. Redrawn and modified from Butler (1992).

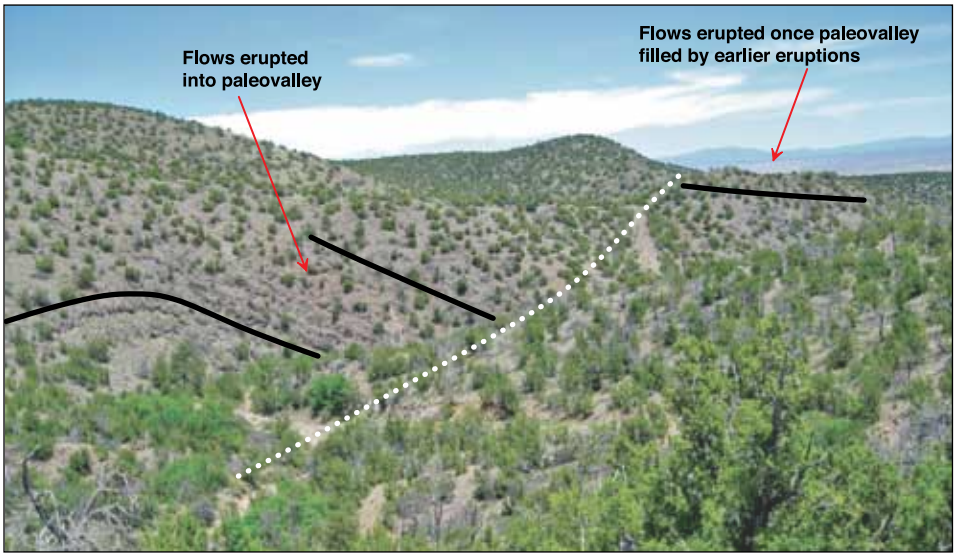


FIGURE 10—View to the northeast along the probable axis of paleovalley within Arroyo de la Plaza Larga. The black lines indicate the average dip of the Lobato basalt flows. Dotted white line is the inferred axis of the paleovalley.

east-down faults near Abiquiu to the west (Koning et al. 2005). Sediment thickness in the Abiquiu embayment is approximately 1 km (0.6 mi), and the geometry of the basin approximates a structural bench (Baldridge et al. 1994) broken by many north-south-trending normal faults (Koning et al. 2005). To the southeast, deep inner grabens of the Española Basin contain basin fill as thick as 3–5 km (1.9–3 mi; Cordell 1978 and cross sections of Kelley 1978; Koning 2003; Koning and Aby 2003; and Koning and Manley 2003). Near the study area, the Santa Clara fault is flanked by a relatively wide zone (hundreds of meters) of moderately to steeply southeast-dipping beds. Vertical displacement across the fault approximates 480–495 m (1,575–1,624 ft) using offset of a Lobato Formation flow (see cross section C–C′ of Koning et al. 2004a, p. 366). The Santa Clara fault and other minor structures appear to have been active at ~11 Ma to 9 Ma and to have influenced erosional and depositional patterns, as some basalt flows dramatically thicken in paleovalleys adjacent to fault scarps in the area (Koning et al. 2005). In the middle Miocene, before 13 Ma, the Española Basin was occupied by two depositional systems influenced by the Santa Clara and Embudo fault systems. Deposits on the west include the fluvial sandstones of Chama–El Rito Member, whereas those on the east are the fluvial deposits of the Dixon Member and lithosome B of Cavazza (1986), both sourced east of the Picuris–Pecos fault in the Sangre de Cristo Mountains. Increased slip along several faults of the Española Basin may have increased the slope of the west-tilted half-graben and shifted the zone of maximum subsidence to the west against the western basin margin (Koning et al. 2004b). Based on the distribution and thickness of sediments before middle Miocene time, the area was generally a broad basin with little evidence of rift-bounding structures significantly influencing sediment deposition (Manley 1982; Baldridge et al. 1994). The depositional setting changed after middle Miocene, and the sediment record reflects the current rift geometry of deep sedimentary basins and structural control of the rift margin and inter-rift fault systems. The emplacement of Lobato Formation into deep paleovalleys adjacent to the Santa Clara fault demonstrates paleorelief across these structures that influenced volcanic flow and sedimentation patterns during the late Miocene. In addition, the dispersion of the site mean directions from the sampled sections are considerably less (k values of 179 and 229; Table 1) than typical for the full range of Neogene paleosecular variation (k ~25), indicating that the flows were emplaced rapidly relative to secular variation. It is probable that the sampled flows were erupted in a time span as short as 100s to 1,000s of years, resulting in the rapid infilling of the paleocanyon adjacent to the Santa Clara fault.

## Conclusions

Lobato Formation volcanism at Arroyo de la Plaza Larga in the southern Española Basin formed from a subduction-modified lithospheric mantle and contributed to precaldera mafic volcanism in the Jemez Mountains volcanic field. Lobato Formation basalts from the Cerro Roman vent flowed across a gently sloping, low- to moderate-relief surface until flowing downslope into a valley created by vertical displacement along the Santa Clara fault. Based on the geometry of the flows, our study estimates that several hundreds of meters of vertical displacement existed along the Santa Clara fault at Arroyo de la Plaza Larga at about 10 m.y. ago. Considering the paleotopographic relief at Arroyo de la Plaza Larga, it is probable

that fault throw estimates for the study area are less than the 480–495 m (1,575–1,624 ft) vertical offsets documented from other locations in the area. Nonetheless, the escarpment influenced depositional patterns in the Española Basin along the western margin of the active Rio Grande rift system before being rapidly filled with the eruption of the Lobato Formation basalts.

## Acknowledgments

We thank Shari Kelley and Dan Koning for introducing us to the Lobato Formation outcrops in Arroyo de la Plaza Larga. We acknowledge New Mexico Highlands University undergraduates Joel Lowry and Louis Garcia for assistance with sample collection and Amanda Aragon and Rachell Pitrucha for assistance with sample preparation. We thank Scott Baldridge and Mark Hudson for their constructive and insightful reviews. We acknowledge the NSF-Western Alliance for Expanded Student Opportunities grant program for partial financial support for this research.

## References

Aldrich, M. J., Jr., 1986, Tectonics of the Jemez lineament in the Jemez Mountains and Rio Grande rift: Journal of Geophysical Research, v. 91, no. B2, pp. 1753–1762.

Aldrich, M. J., Jr., and Dethier, D. P., 1990, Stratigraphic and tectonic evolution of the northern Española Basin, Rio Grande rift, New Mexico: Geological Society of America, Bulletin, v. 102, pp. 1695–1705.

Bachman, G. O., and Mehnert, H. H., 1978, New K-Ar dates and the late Pliocene to Holocene geomorphic history of the central Rio Grande region, New Mexico: Geological Society of America, Bulletin, v. 89, no. 2, pp. 283–292.

Bailey, R. A., Smith, R. L., and Ross, C. S., 1969, Stratigraphic nomenclature of volcanic rocks in the Jemez Mountains, New Mexico: U.S. Geological Survey, Bulletin 1274-P, 19 pp.

Baldridge, W. S., 2004, Pliocene–Quaternary volcanism in New Mexico and a model for genesis of magmas in continental extension; *in* Mack, G. H., and Giles, K. E. (eds.), The geology of New Mexico, a geologic history: New Mexico Geological Society, Special Publication 11, pp. 313–330.

Baldridge, W. S., Bartov, Y., and Kron, A., 1983, Geologic map of the Rio Grande rift and southeastern Colorado Plateau, New Mexico and Arizona: American Geophysical Union, scale 1:500,000.

Baldridge, W. S., Olsen, K. H., and Callender, J. F., 1984, Rio Grande rift—problems and perspectives; *in* Baldridge, W. S., Dickerson, P. W., Riecker, R. E., and Zidek, J. (eds.), Rio Grande rift—northern New Mexico: New Mexico Geological Society, Guidebook 35, pp. 1–12.

Baldridge, W. S., Damon, P. E., Shafiqullah, M., and Bridwell, R. J., 1980, Evolution of the Rio Grande rift, New Mexico—new potassium-argon ages: Earth and Planetary Science Letters, v. 51, no. 2, pp. 309–321.

Baldridge, W. S., Ferguson, J. F., Braile, L. W., Wang, B., Eckhardt, K., Evans, D., Schultz, C., Gilpin, B., Jiracek, G., and Biehler, S., 1994, The western margin of the Rio Grande rift in northern New Mexico—an aborted boundary?: Geological Society of America, Bulletin, v. 105, pp. 1538–1551.

Barghoorn, S., 1981, Magnetic-polarity stratigraphy of the Miocene type Tesuque Formation, Santa Fe Group, in the Española Valley, New Mexico: Geological Society of America, Bulletin, v. 92, pp. 1027–1041.

Brown, L. L., and Golombek, M. P., 1985, Tectonic rotations within the Rio Grande rift—evidence from paleomagnetic studies: Journal of Geophysical Research, v. 90, no. B1, pp. 790–802.

Brown, L. L., and Golombek, M. P., 1986, Block rotations in the Rio Grande rift, New Mexico: Tectonics, v. 5, no. 3, pp. 423–438, doi: 10.1029/TC005i003p00423.

Butler, R. F., 1992, Paleomagnetism—magnetic domains to geologic terranes: Blackwell Scientific Publications, Boston, 319 pp.

Cavazza, W., 1986, Sedimentation pattern of the rift-filling unit, Tesuque Formation (Miocene), Española Basin, Rio Grande rift, New Mexico: Journal of Sedimentary Petrology, v. 59, no. 2, pp. 287–296.

Chapin, C. E., 1988, Axial basins of the northern and central Rio Grande rifts; *in* Sloss, L. L. (ed.), Sedimentary cover—North American craton, U.S.: Geological Society of America, Geology of North America, v. D–2, pp. 165–170.

Chapin, C. E., and Cather, S. M., 1994, Tectonic setting of the axial basins of northern and central Rio Grande rift; *in* Keller, G. R., and Cather, S. M. (eds.), Basins of the Rio Grande rift—structure, stratigraphy, and tectonic setting: Geological Society of America, Special Paper 291, pp. 5–25.

Chapin, C. E., and Seager, W. R., 1975, Evolution of the Rio Grande rift in Socorro and Las Cruces areas; *in* Seager, W. R., Clemons, R. F., and Callender, J. F. (eds.), Las Cruces country: New Mexico Geological Society, Guidebook 26, pp. 297–321.

Cordell, L., 1978, Regional geophysical setting of the Rio Grande rift: Geological Society of America, Bulletin, v. 89, no. 7, pp. 1073–1090.

Cox, A., and Doell, R. R., 1960, Review of paleomagnetism: Geological Society of America, Bulletin, v. 71, pp. 645–768.

Dalrymple, G., Cox, G., Doell, R., and Gromme, C., 1967, Pliocene geomagnetic polarity epochs: Earth and Planetary Science Letters, v. 2, pp. 163–173.

Dethier, D. P., and Manley, K., 1985, Geologic map of the Chili quadrangle, Rio Arriba County, New Mexico: U.S. Geological Survey, Miscellaneous Field Studies Map MF-1814, scale 1:24,000.

Dethier, D. P., Aldrich, M. J., Jr., and Shafiqullah, M., 1986, New K-Ar ages for Miocene volcanic rocks from the northeastern Jemez Mountains and Tejana Mesa, New Mexico: Isochron/West, no. 47, pp. 12–14.

Dungan, M. A., Muehlberger, W. R., Leininger, L., Peterson, C., McMillan, N. J., Gunn, G., Lindstrom, M., and Haskin, L., 1984, Volcanic and sedimentary stratigraphy of the Rio Grande gorge and the late Cenozoic geologic evolution of the southern San Luis Valley; *in* Baldridge, W. S., Dickerson, P. W., Riecker, R. E., and Zidek, J. (eds.), Rio Grande rift—northern New Mexico: New Mexico Geological Society, Guidebook 35, pp. 157–170.

Dunlop, D. J., and Özdemir, O., 1997, Rock magnetism—fundamentals and frontiers, Cambridge studies in magnetism, 3: Cambridge University Press, New York, 573 pp.

Everitt, C. W. F., and Clegg, J. A., 1962, A field test of paleomagnetic stability: Geophysical Journal of London, v. 6, pp. 312–319.

Gardner, J. N., Goff, F., Garcia, S., and Hagan, R. C., 1986, Stratigraphic relations and lithologic variations in the Jemez volcanic field, New Mexico: Journal of Geophysical Research, v. 91, no. B2, pp. 1763–1778.

Goff, F., Gardner, J. N., Baldridge, W. S., Hulen, J. B., Nielson, D. L., Vaniman, D., Heiken, G., Dungan, M. A., and Broxton, D., 1989, Excursion 17B: Volcanic and hydrothermal evolution of Valles caldera and Jemez volcanic field; *in* Chapin, C. E., and Zidek, J. (eds.), Field excursions to volcanic terrains in the western United States, Volume I, Southern Rocky Mountain region: New Mexico Bureau of Mines and Mineral Resources, Memoir 46, pp. 381–434.

Gonzales, M. A., 1993, Geomorphic and neotectonic analysis along a margin of the Colorado Plateau and Rio Grande rift in northern New Mexico: Unpublished Ph.D. dissertation, University of New Mexico, Albuquerque, 302 pp.

Harlan, S. S., and Geissman, J. W., 2009, Paleomagnetism of Tertiary intrusive and volcaniclastic rocks of the Cerrillos Hills and surrounding region, Española Basin, New Mexico, U.S.A.—assessment and implications of vertical-axis rotations associated with extension of the Rio Grande rift: Lithosphere, v. 1, no. 3, pp. 155–173, doi: 10.1130/L53.1.

Harrington, C. D., and Aldrich, M. J., Jr., 1984, Development and deformation of Quaternary surfaces on the northeastern flank of the Jemez Mountains; *in* Baldridge, W. S., Dickerson, P. W., Riecker, R. E., and Zidek, J. (eds.), Rio Grande rift—northern New Mexico: New Mexico Geological Society, Guidebook 35, pp. 235–239.

Hrouda, F., 2003, Indices for numerical characterization of the alteration processes of magnetic minerals taking place during investigation of temperature variation of magnetic susceptibility: Studia Geophysica et Geodaetica, v. 47, pp. 847–861.

Hudson, M. R., Thompson, R. A., Barba, K. E., Minor, S. A., and Warren, R. G., 2004, Counterclockwise declination anomaly in paleomagnetism of the Pliocene Cerros del Rio volcanic field, New Mexico—an expression of late Rio Grande rift distributed shear? (abs.): Geological Society of America, Abstracts with Programs, v. 36, no. 5, p. 436.

Irvine, T. N., and Baragar, W. R. A., 1971, A guide to the chemical classification of the common volcanic rocks: Canadian Journal of Earth Sciences, v. 8, no. 5, pp. 523–548.

Kelley, V. C., 1978, Geology of Española Basin, New Mexico: New Mexico Bureau of Mines and Mineral Resources, Geologic Map 48, scale 1:125,000.

Kelson, K. I., Unruh, J. R., and Bott, J. D. J., 1997, Field characterization, kinematic analysis, and initial paleoseismic assessment of the Embudo fault, northern New Mexico: Final Technical Report to the U.S. Geological Survey from William Lettis and Associates, Inc., 48 pp.

Kirschvink, J. L., 1980, The least-square line and plane and the analysis of paleomagnetic data—examples from Siberia and Morocco: Geophysical Journal of the Royal Astronomical Society, v. 62, pp. 699–718.

Koning, D. J., 2003, Geology of the Chimayo 7.5-minute quadrangle, Rio Arriba and Santa Fe Counties, New Mexico: New Mexico Bureau of Geology and Mineral Resources, Open-file Geologic Map 71, scale 1:24,000, online at http://geoinfo.nmt.edu/publications/maps/geologic/ofgm/details.cfml?Volume=71.

Koning, D. J., and Aby, S., 2003, Geology of the Velarde 7.5-minute quadrangle, Rio Arriba and Taos Counties, New Mexico: New Mexico Bureau of Geology and Mineral Resources, Open-file Geologic Map 79, scale 1:24,000, online at http://geoinfo.nmt.edu/publications/maps/geologic/ofgm/details.cfml?Volume=79.

Koning, D. J., and Manley, K., 2003, Geology of the San Juan Pueblo 7.5-minute quadrangle, Rio Arriba and Santa Fe Counties, New Mexico: New Mexico Bureau of Geology and Mineral Resources, Open-file Geologic Map 70, scale 1:24,000, online at http://geoinfo.nmt.edu/publications/maps/geologic/ofgm/details.cfml?Volume=70.

Koning, D. J., Aby, S. B., and Dunbar, N., 2004a, Middle-upper Miocene stratigraphy of the Velarde graben, north-central New Mexico: tectonic and paleogeographic implications; *in* Brister B., Bauer, P. W., Read, A. S., and Lueth, V. W. (eds.), Geology of the Taos region: New Mexico Geological Society, Guidebook 55, pp. 359–373.

Koning, D. J., Ferguson, J. F., Paul, P. J., and Baldridge, W. S., 2004b, Geologic structure of the Velarde graben and the southern Embudo fault system, north-central N.M.; *in* Brister B., Bauer, P. W., Read, A. S., and Lueth, V. W. (eds.), Geology of the Taos region: New Mexico Geological Society, Guidebook 55, pp. 158–171.

Koning, D. J., Skotnicki, S., Kelley, S. A., and Moore, J., 2005, Preliminary geologic map of the Chili 7.5-minute quadrangle, Rio Arriba County, New Mexico: New Mexico Bureau of Geology and Mineral Resources, Open-file Geologic Map 103, scale 1:24,000, online at http://geoinfo.nmt.edu/publications/maps/geologic/ofgm/details.cfml?Volume=103.

Leininger, R. L., 1982, Cenozoic evolution of the southernmost Taos Plateau, New Mexico: Unpublished M.S. thesis, University of Texas at Austin, 110 pp.

Loeffler, B. M., Vaniman, D. T., Baldridge, W. S., and Shafiqullah, M., 1988, Neogene rhyolites of the northern Jemez volcanic field, New Mexico: Journal of Geophysical Research, v. 93, no. B6, pp. 6157–6167.

Luedke, R., and Smith, R., 1978, Map showing distribution, composition and age of late Cenozoic volcanic centers in Arizona and New Mexico: U.S. Geological Survey, Miscellaneous Investigations Map I-1091-A, scale 1:1,000,000.

Mankinen, E. A., Larson, E. E., Gromme, C. S., Prevot, M., and Coe, R. S., 1987, The Steens Mountain (Oregon) geomagnetic polarity transition 3. Its regional significance: Journal of Geophysical Research, v. 92, no. B8, pp. 8057–8076, doi: 10.1029/JB092iB08p08057.

Manley, K. 1979, Stratigraphy and structure of the Española Basin, Rio Grande rift, New Mexico; *in* Riecker, R. E. (ed.), Rio Grande rift—tectonics and magmatism, American Geophysical Union, pp. 71–86.

Manley, K., 1982, Geologic map of the Cañones quadrangle, Rio Arriba County, New Mexico: U.S. Geological Survey, Miscellaneous Field Studies Map MF-1440, scale 1: 24,000.

Manley, K., and Mehnert, H. H., 1981, New K-Ar ages for Miocene and Pliocene volcanic rocks in the northwestern Española Basin and their relationships to the history of the Rio Grande rift: Isochron/West, no. 30, pp. 5–8.

Mayo, E. B., 1958, Lineament tectonics and some ore districts of the Southwest: American Institute of Mining, Metallurgical, and Petroleum Engineers, Transactions, v. 211, pp. 1169–1175.

McMillan, N. J., 1998, Temporal and spatial magmatic evolution of the Rio Grande rift; *in* Mack, G. , Austin, G. S., and Barker, J. M. (eds.), Las Cruces country II: New Mexico Geological Society, Guidebook 49, pp. 107–116.

Moskowitz, B. M., 1981, Methods of estimating Curie temperatures of titanomagnetites from experimental Js-T data: Earth and Planetary Science Letters, v. 53, pp. 84–88.

Muehlberger, W. R., 1978, Frontal fault zone of northern Picuris Range; *in* Hawley, J. W., (comp.), Guidebook to Rio Grande rift in New Mexico and Colorado: New Mexico Bureau of Mines and Mineral Resources, Circular 163, pp. 44–45.

Muehlberger, W. R., 1979, The Embudo fault between Pilar and Arroyo Hondo, New Mexico—an active intracontinental transform fault; *in* Ingersoll, R. V., Woodward, L. A., and James, H. L. (eds.), Guidebook of Santa Fe country: New Mexico Geological Society, Guidebook 30, pp. 77–82.

Nakamura, N. 1974, Determination of REE, Ba, Fe, Mg, Na, and K in carbonaceous and ordinary chondrites: Geochimica et Cosmochemica Acta, v. 38, pp. 757–775.

Olsen, K. H., Baldridge, W. S., and Callender, J. F., 1987, Rio Grande rift—an overview: Tectonophysics, v. 143, pp. 119–139.

Özdemir, O., and O'Reilly, W., 1981, High-temperature hysteresis and other magnetic properties of synthetic monodomain titanomagnetites: Physics of the Earth and Planetary Interiors, v. 25, pp. 406–418, doi:10.1016/0031-9201(81)90052-2.

Özdemir, O., and O'Reilly, W., 1982, Magnetic hysteresis properties of synthetic monodomain titanomaghemites: Journal of Geomagnetism and Geoelectricity, v. 34, pp. 467–478.

Pearce, J. A., 1983, Role of sub-continental lithosphere in magma genesis at active continental margins; *in* Hawkesworth, C. J., and Norry, M. J. (eds.), Continental basalts and mantle xenoliths: Shiva, UK, pp. 230–249.

Pearce, J. A., and Cann, J. R., 1973, Tectonic setting of basic volcanic rocks determined using trace element analyses: Earth and Planetary Science Letters, v. 19, pp. 290–300.

Personius, S. F., and Machette, M. N., 1984, Quaternary and Pilocene faulting in the Taos Plateau region, northern New Mexico; *in* Baldridge, W. S., Dickerson, P. W., Riecker, R. E., and Zidek, J. (eds.), Rio Grande rift—northern New Mexico: New Mexico Geological Society, Guidebook 35, pp. 83–90.

Petronis, M. S., O'Driscoll, B., and Lindline, J., 2011, Late stage oxide growth associated with hydrothermal alteration of the Western Granite, Isle of Rum, NW Scotland: Geochemistry, Geophysics, Geosystems, v. 12, Q01001, doi: 10.1029/2010GC003246.

Rosendahl, B. R., 1987, Architecture of continental rifts with special reference to East Africa: Annual Review of Earth and Planetary Sciences, v. 15, pp. 445–503.

Roy, J. L., and Park, J. K., 1974, The magnetization process of certain red beds—vector analysis of chemical and thermal results: Canadian Journal of Earth Sciences, v. 2, pp. 437–471.

Russell, J. K., and Nicholls, J., 1988, Analysis of petrologic hypotheses with Pearce element ratios: Contributions to Mineralogy and Petrology, v. 99, pp. 25–35.

Russell, J. K., and Stanley, C. R. (eds.), 1990, Theory and application of Pearce element ratios to geochemical data analysis: Geological Association of Canada, Short Course, v. 8, 315 pp.

Salyards, S. L., Ni, J. F., and Aldrich, M. J., Jr., 1994, Variation in paleomagnetic rotations and kinematics of the north-central Rio Grande rift, New Mexico; *in* Keller, G. R., and Cather, S. M. (eds.), Basins of the Rio Grande rift—structure, stratigraphy, and tectonic setting: Geological Society of America, Special Paper 291, pp. 59–71.

Singer, B. S., and Kudo, A. M., 1986, Assimilation-fractional crystallization of Polvadera Group rocks in the northwestern Jemez Mountains volcanic field, New Mexico: Contributions to Mineralogy and Petrology, v. 94, pp. 374–386.

Steinpress, M. G., 1980, Neogene stratigraphy and structure of the Dixon area, Española Basin, north-central New Mexico: Unpublished M.S. thesis, University of New Mexico, Albuquerque, 127 pp., plus 2 plates.

Steinpress, M. G., 1981, Neogene stratigraphy and structure of the Dixon area, Española Basin, north-central New Mexico: Geological Society of America, Bulletin, Part II, v. 91, no. 12, pp. 2553–2671.

Smith, H. T. U., 1938, Tertiary geology of the Abiquiu quadrangle, New Mexico: Journal of Geology, v. 46, pp. 933–965.

Tauxe, L., 1998, Paleomagnetic principles and practice, vol. 17 of *Modern approaches in geophysics*: Kluwer Academic Publishers, Dordrecht, Boston, London.

Wilson, A. D., 1955, A new method for the determination of ferrous iron in rocks and minerals: Bulletin of the Geological Survey of Great Britain, v. 9, pp. 56–68.

Wolff, J. A., Rowe, M. C., Teasdale, R., Gardner, J. N., Ramos, F. C., and Heikoop, C. E., 2005, Petrogenesis of pre-caldera mafic lavas, Jemez Mountains volcanic field (New Mexico, USA): Journal of Petrology, v. 46, no. 2, pp. 407–439.

Zijderveld, J. D. A., 1967, A.C. demagnetization of rocks—analysis of results; *in* Collinson, D. W., Creer, K. M., and Runcorn, S. K. (eds.), Methods in Paleomagnetism: Elsevier, Amsterdam, pp. 254, 286.

## Some abbreviations used in this paper

| | |
|---|---|
| AF | alternating field, as in "AF demagnetization" |
| A/m | ampere/meter |
| BIRM | backfield isothermal remanent magnetization |
| ChRM | characteristic remanent magnetization |
| DC | direct current |
| IRM | isothermal remanent magnetization |
| MDF | median destructive field |
| MORB | modern mid-ocean ridge basalts |
| mT | millitesla |
| NRM | natural remanent magnetization |
| PSD | pseudosingle domain |
| SD | single domain |
| SIRM | saturation isothermal remanent magnetization |
| T | tesla |
| TH | thermal, as in "TH demagnetization" |
| TRM | thermal remanent magnetization |
| VRM | viscous remanent magnetization |